RSC Advances

RSC Advances

www.rsc.org/advances

ROYAL SOCIETY OF CHEMISTRY

www.rsc.org/advances

Journal Name

ARTICLE

Enhanced photoelectrochemical and photocatalytic performance of iodine-doped titania nanotube arrays

Katarzyna Siuzdak,[a] Mariusz Szkoda,[b] Mirosław Sawczak,[a] Anna Lisowska-Oleksiak,[b]

Jakub Karczewski[c] and Jacek Ryl[d]

The paper discusses the synthesis and performance of iodine doped titania nanotube arrays exhibited under irradiation. The doping procedure was performed as an additional, electrochemical process carried out after formation of nanotube arrays *via* anodization of Ti substrate. The optical and structural properties were characterized using Raman, UV-vis, photoluminescence and X-ray photoelectron spectroscopy. The surface morphology and cross-section studies performed by means of the scanning electron microscopy show that the ordered tubular architecture is not influenced by doping method. However, iodine doping causes a reduction of bandgap energy and photoluminescence intensity. The nanotubular TiO_2 electrodes have been monitored by electrochemical (using cyclic voltammetry and electrochemical impedance spectroscopy) and in-situ UV-vis spectroelectrochemical measurements in contact with an aqueous electrolyte. Collected results show significant differences in electrochemical activity between pure and doped titania exhibited as i.e. change of Mott-Schottky relation or shift in the onset potential when a decrease in reflectance is initiated. The photocurrent density reached 155.2 and 142.2 $\mu A\ cm^{-2}$ for iodine doped materials when KI and HIO_4 were used as iodine precursors whereas only 25.6 $\mu A\ cm^{-2}$ was registered for pure titania nanotubes under UV-vis illumination. Moreover, doped samples are far more efficient at the photodegradation progress than undoped material leading to decomposition of over 70% of methylene blue used as a model organic pollution. Reported studies demonstrate for the first time the detailed optical, electrochemical and photoelectrochemical studies of iodine doped nanotube arrays.

A Introduction

Highly ordered titania nanotube arrays have attracted worldwide attention in different fields of science and industrial technology because of a significant number of potential applications enabled by the electric, ionic, absorbance and biomedical properties of nanotubes.[1] In comparison to TiO_2 nanoparticles, tubular architecture allows, e.g. for a non-disturbed charge transport along the tube wall and specific light capture inside the pores.[2] Titania nanotubes possessing a large surface area, characterized by strong mechanical strength and perfect alignment are regarded as materials of great scientific and practical concern. Such nanostructures could be achieved using the anodization technique, known as one of the cheapest, straight-forward and simplest

synthesis method resulting in the highly ordered material.[3] Furthermore, the structure of titania nanotubes formed during the anodization process could be easily controlled by changing the anodization potential, temperature, and electrolyte composition or geometry of the electrolytic cell.[4,5] Until now, layers composed of TiO_2 nanotube arrays have been successfully used in dye-sensitized solar cells,[6] gas sensors,[7] as a photocatalyst[8] or membrane for protein separation and drug delivery[9]. However, nanotube activity in processes carried out under illumination is limited by their wide bandgap E_{bg} that corresponds to ultraviolet light[10]. While the large E_{bg} is crucial for many applications, it limits the use of solar-irradiated driven applications, because only 5% of the total sun spectra are provided in the UV range. Therefore, different strategies were proposed in order to shift the activity of titania towards longer wavelengths. Bandgap engineering is mainly based on bulk doping or surface modification.[11] Among them, non-metal doping is regarded as simple, providing material that is stable and highly active under visible light illumination. For intentional doping of titania nanotubes: nitrogen,[12] sulfur,[13] phosphorus,[14] boron[15] and iodine[16] atoms were proposed as favorable non-metallic candidates. Taking into account the number of scientific reports, nitrogen and boron are the most popular dopant atoms and their presence in the structure of titania results in a highly active material, whereas studies on other possible non-metal dopant

[a] *Centre of Plasma and Laser Engineering, Szewalski Institute of Fluid-Flow Machinery, Polish Academy of Sciences, Fiszera 14, Gdańsk 80-231, Poland; Fax: +48 58 3416144; Tel: +48 58 6995294; *e-mail: ksiuzdak@imp.gda.plAddress here.*

[b] *Department of Chemistry and Technology of Functional Materials, Chemical Faculty, Gdańsk University of Technology, Narutowicza 11/12, Gdańsk 80-233, Poland*

[c] *Faculty of Applied Physics and Mathematics, Gdańsk University of Technology, Narutowicza 11/12, 80-233 Gdańsk, Poland*

[d] *Department of Electrochemistry, Corrosion and Materials Engineering, Gdańsk University of Technology, Narutowicza 11/12, 80-233 Gdańsk, Poland*

atoms are not widespread. Until now, no electrochemical investigation including registration of transient photocurrent under UV-vis illumination or impedance studies has been performed for the iodine doped TiO_2.[16,17] Such research enables a description of redox properties that are among the most important features of any functional material for solar energy utilization involving photocatalysis and photovoltaics. Depending on the crystal structure, particle size, doping level, surface modification, environment, titanium dioxide as with any other semiconducting material is characterized by unique potentials of band edges. Thus, in order to make a comprehensive characterization of the semiconductor, great effort should be made to ensure a proper determination of potentials of band edges. As it is known, in the absence of external filed, the interface of the semiconductor with an aqueous electrolyte solution is usually characterized by band bending caused by adjustment of the Fermi level with the corresponding energy level in solution.[18] However, at a certain potential applied to the semiconducting electrode, the Fermi level lies at the same energy as the solution redox potential. There is no net transfer of charge and band bending does not occur.[19] Such potential is described as flat-band potential (E_{fb}) and because E_{fb} for an n-type semiconductor lies at the vicinity of the conduction band (CB), the position of CB can be then estimated. Two different approaches are known that can be used for flat-band determination, referring to the excited or not-excited state of the semiconductor. In the first case, during the measurement, the sample is irradiated and in fact the potential of the quasi-Fermi level is determined that is useful for the photocatalytic processes.[20,21,22,23] However, information about the redox properties of the semiconductor in its ground state can only be achieved without its light-driven excitation. Such conditions are met during electrochemical impedance spectroscopy and spectroelectrochemical measurements. In the case of pure and doped titanium dioxide nanotubes, the Mott-Schottky analysis of impedance data has already been used for flatband determination,[24] whereas spetroelectrochemical measurements have been conducted only for semitransparent electrodes composed of thin layer of TiO_2 nanoparticles.[25,26,27] According to Świętek et al.,[28] spectroelectrochemical determination of flat-band potential could be also successfully applied for non-transparent materials using diffuse reflectance spectroscopy combined together with electrochemical measurements. The tracking of changes in reflectance, that is strongly related to electron density in the conduction band, enables determination of the potential at which the electrochemical reduction of the semiconductor is initiated. However, until now this technique has not been used for the characterization of redox properties of titania nanotubes. Additionally, any comparison between two different approaches in determination of E_{fb} position: a) based on electrochemical impedance spectroscopy and b) spectroelectrochemical measurement, to date has not been performed, analyzed and discussed.

Here, we report preparation of iodine doped titanium dioxide nanotube arrays *via* electrochemical process carried out on biased as-anodized titania plates immersed in KI or HIO_4 solution. Materials were characterized using various spectroscopic techniques: UV-vis, Raman, photoluminescence and X-ray

photoelectron spectroscopy. Morphology, together with the elemental analysis, was studied using SEM equipped with EDX. The photocatalytic activity of nanotube array films was tested for the degradation of methylene blue as a model organic pollutant. A significant part of the research was focused on electrochemical characterization covering voltammetry as well as impedance measurements and spectroelectrochemical studies. Great attention has been paid to a discussion of flat-band potential determined using two different methods without exposition of studied material to simulated solar radiation: the first one based on electrochemical impedance spectroscopy and the second one based on an UV-vis spectroelectrochemical measurement. Moreover, the current response registered under both vis and UV-vis illumination for iodine doped titania was compared to that of pure TiO_2 nanotubes.

B Experimental

Material preparation

Titania nanotubes were prepared via a two-step electrochemical anodization of analytical grade Ti plate (Steam, 99.7%) in a fluoride-containing solution. The procedure leading to formation of TiO_2 nanotubes was described in our previous report.[12] To sum it up briefly, it is based on a two-stage anodization process that provides highly ordered nanotubular architecture.[5] The first and the second step were performed at the same temperature conditions (23°C ± 1°C), electrolyte composition (0.27 M NH_4F in 1%/99% v/v water/ethylene glycol solution) and anodization parameters (40 V, 2 h). Before the second anodization, the nanotubular layer formed during the first step was removed by overnight etching in a 0.5% wt. solution of oxalic acid. At the end of the entire anodization process, titanium plates covered with nanotubes were ultrasonically cleaned in 0.05% wt. HF for 60 s, in order to remove surface debris.

Iodine doping was realized similarly to Su et al.[16] *via* an electrochemical process in a two-electrode arrangement in two types of electrolytes: 0.1 M solution of potassium iodide or periodic acid. When the periodic acid solution was used, the as-anodized titania nanotubes served as the cathode and a platinum mesh as the anode. On the contrary, when the solution of potassium iodide was applied as an electrolyte, the setting of Ti plate covered by TiO_2 nanotubes and a platinum mesh were interchanged and they served as an anode and a cathode respectively. After optimization procedure, electrochemical doping was performed for 15 min. at 1.5 V (23°C ± 1°C). According to the chemical formula of iodine precursors used, the titania nanotube samples were coded as: I-TiO_2-KI and I-TIO_2-HIO_4. Finally, samples were rinsed with deionized water and annealed at a temperature of 450°C for 2 h (heating rate: 2°C min^{-1}) in order to process conversion into the crystalline phase. Pure, ordered TiO_2 nanotube arrays obtained after two-step anodization and a calcination process were used as a reference sample. Therefore, the only difference in the preparation procedure of pure and doped titania was the electrochemical doping step.

Characterization

The morphology and cross-section of the samples were investigated by the Schottky field emission scanning electron microscopy (FEI

Quanta FEG 250) with ET secondary electron detector. Beam accelerating voltage was kept at 10 kV. For elemental analysis, the Energy Dispersive X-ray Spectroscopy was performed by EDAX Genesis APEX 2i with ApolloX SDD spectrometer in a particular area of each sample.

The UV-Vis reflectance spectra of titania nanotubes were measured with a dual beam UV-Vis spectrophotometer (Lambda 35, Perkin-Elmer) equipped with a diffuse reflectance accessory. The spectra were registered in a range of 300 - 900 nm, with a scanning speed of 240 nm/min. Bandgap energy values were determined as the intercept of the tangent of the plot of transformation of the Kubelka-Munk function ($KM^{0.5}E_f^{0.5}$) vs. photon energy, where $KM = (1-R)^2/2R$, R – the intensity of radiation reflected from the sample. This method is commonly used for both pure and doped titania nanotube arrays.

The Raman spectra were recorded by a confocal micro-Raman spectrometer (InVia, Renishaw) with sample excitation, by means of an argon ion laser emitting at 514 nm operating at 5% of its total power (50 mW).

The photoluminescence (PL) measurements were carried out using laboratory setup consisting of 0.3 m Czerny-Turner spectrograph (SR303i, Andor) equipped with ICCD camera (DH740, Andor). Samples of pure and doped TiO_2 were excited with UV LED (365 nm center wavelength, 9 nm FWHM, 350 mW output power). The excitation radiation, focused by quartz lens, was directed onto the sample surface at an angle of 45°. Additionally, the band-pass filter (UG11, Schott) was applied between the excitation source and the sample to block UV LED radiation above 380 nm. The fluorescence signal was collected perpendicularly to the sample surface using a microscope objective and focused on the entrance of the optical fiber. In the detection path, the band-pass filters (GG44, Schott) were used for blocking the excitation radiation.

Escalab 250Xi from ThermoFisher Scientific was used to carry out high-resolution x-ray photoelectron spectroscopy (XPS) measurements to determine chemical binding properties of the surface, utilizing monochromatic Al Kα source with charge neutralization implemented by means of a flood gun. High-resolution spectra were recorded at energy step size of 0.1 eV at a pass energy of 10 eV. In order to normalize spectroscopic measurements, X axis (binding energy, E_{bin}) from XPS spectrum was calibrated for peak characteristics of neutral carbon 1s ($E_{bin} = 284.6$ eV). Data analysis was performed using Avantage software provided by the manufacturer.

Electrochemical characterization

The electrochemical studies of pure and iodine-doped titania nanotubes (cyclic voltammetry: CV, linear sweep voltammetry LV, electrochemical impedance spectroscopy EIS) were conducted using an AutoLab PGStat 302N potentionstat-galvanostat system (Methrom, Autolab) in the standard three-electrode assembly, where titanium foil covered by nanotubes served as a working electrode (active surface area of 0.4 cm^2). The Pt mesh was used as a counter electrode, while Ag/AgCl/0.1M KCl as a reference electrode. All electrochemical tests were carried out in 0.1 M K_2SO_4 that was extensively purged with argon gas for about 1 h. Ar-

cushion above the electrolyte was applied during the measurements.

Electrochemical impedance spectroscopy measurements were conducted at the frequency range from 20 kHz to 0.1 Hz, covering 75 points and with 10 mV amplitude of the AC signal. In order to perform the Mott-Schottky analysis, impedance spectra were recorded at different potentials in the range from +0.6 V to - 0.5 V vs. Ag/AgCl/0.1M KCl. Before each spectra registration, the potential was held to achieve a steady state condition. The impedance data were analyzed on the basis of an electric equivalent circuit (EEQC) using an EIS Spectrum Analyser[29] program. The modified Powell algorithm[30] was used with amplitude weighting r_a:

$$r_a(\omega, P_1...P_M) = r_c^2/(N-M) \tag{1}$$

where N is the number of points, M is the number of parameters, ω is the angular frequency, $P_1...P_M$ are parameters. Parameter r_c is defined as

$$r_c^2 = \sum_{i=1}^{N} \frac{\left(Z_i^{'} - Z_{i_{calc}}^{'}\right)^2 + \left(Z_i^{''} - Z_{i_{calc}}^{''}\right)^2}{Z_i^{'2} + Z_{i_{calc}}^{'}{}^2} \tag{2}$$

where i corresponds to the measured values of impedance and i_{calc} is attributed to the calculated values; N is the number of points.

Photoactivity characterization

Measurements carried out under illumination were performed in the photoelectrochemical cell equipped with a quartz window and the cooling jacket keeping constant temperature at 23°C (±1°C) provided by thermostat (Julabo F-12) control. The photocurrent (linear voltammetry and chronoampertometry) measurements were carried out at + 0.5 V vs. Ag/AgCl/0.1M KCl bias voltage. A high-pressure 150 W xenon lamp (Osram XBO 150) equipped with AM1.5 filter and the automated light chopper with a period of 20 s was used as a light source. The light intensity was adjusted to 100 mW cm^{-2} (controlled by powermeter, Ophir). In order to perform measurements in the visible light range, the additional cut-off optical filter (λ > 420 nm) was added to the experimental setup.

UV-vis in-situ spectroelectrochemical measurements were carried out using a UV-Vis spectrophotometer (Lambda 35, Perkin-Elmer) equipped with a diffuse reflectance accessory. More detailed description of in-situ measurements were described in electronic supplementary information. As an electrochemical cell, quartz cuvette was used. The titanium plate covered with a nanotubes layer served as a working electrode. The Ag/AgCl wire was used as a reference electrode. The relationship between this pseudoelectrode and Ag/AgCl/0.1M KCl used in 0.1M K_2SO_4 is expressed as: E vs. Ag/AgCl/0.1MKCl = E vs. Ag/AgCl + 0.158 V. The changes in reflectance were registered together with simultaneous potential changes of the working electrode from +0.2 V to -0.9 V vs. Ag/AgCl. The scan rate was established at 1 mV s^{-1} and the changes in reflectance were registered at 550 nm that stayed as a wavelength at which maximum in absorbance is observed in the visible range. Similarly to results reported by Świętek et al.[28], the decrease in the scan rate below 1 mVs^{-1} did not result in further changes of the onset potential.

The photocatalytic activity of the materials was tested for the degradation of methylene blue solution (MB), under a xenon lamp

(Osram XBO 150) equipped with AM1.5 filter. A titanium plate covered by pure and doped nanotube arrays with the surface area of 2.5 cm^2 was immersed in methylene blue solution and exposed to irradiation. The initial concentration of MB was 10 μmol/dm^3 (C_0). The concentration of MB during decomposition (C) was monitored every 10 min. using a Lambda 35 UV-VIS spectrophotometer (Perkin Elmer). The blank experiment was carried out under the same conditions without a catalyst.

B Results and discussion

Morphology and structure characterization

Fig. 1 shows the top-view morphologies of the pure and doped titania nanotube arrays prepared by means of the anodization process. Obtained uniform layers are formed from highly ordered and aligned tubes. When comparing SEM images registered for all materials, no difference in architecture was observed. Thus, electrochemical doping does not affect the morphology and only the presence of dopant atoms can have an impact on the properties and the electrochemical performance of materials. Images registered at higher magnification (see Fig. 2 a) allow the determination of tube dimensions: 95 nm in diameter and 37 nm of wall thickness in the top level. As it can be seen in Fig. 2b, the thickness of tube walls gradually increases from top to bottom of the layer (see the area marked by the white circle, Fig. 2b) that is described usually as V-shape morphology.[1] This is due to the exposure of as-formed tubes to the etching fluoride ion-rich environment. According to Yasuda et al.,[31] the wall thickness is smaller at the level close to the nanotube top, since this part is exposed to the electrolyte for a longer period of time.
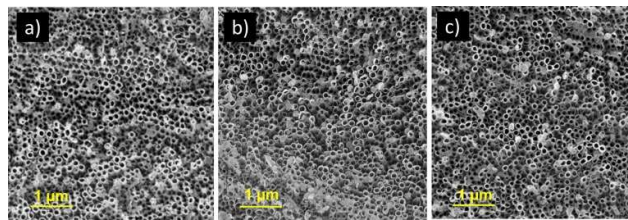

Fig. 1 Surface SEM image of titania nanotube arrays:
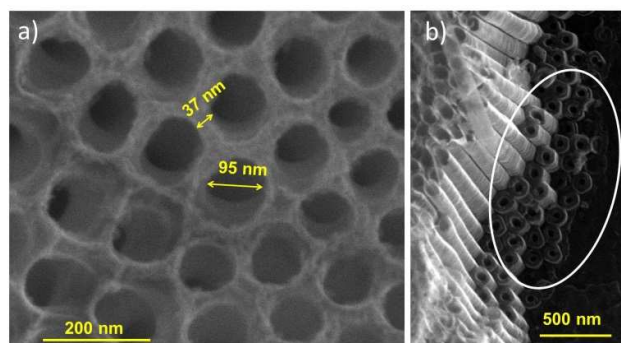a) pure, b) I-TiO$_2$-KI and c) I-TiO$_2$-HIO$_4$.

Fig. 2 High resolution SEM image of I-TiO$_2$-HIO$_4$ nanotube arrays.

As it can be seen in Fig. 3, cross-section images for both types of iodine doped TiO$_2$ together with EDX analysis at the top and at the

bottom level of the titania layer were registered. The tube length for I-TiO$_2$-KI and I-TiO$_2$-HIO$_4$ was 2.2 μm. Apart from the titanium and oxygen, iodine was detected on the same level at the base and at the surface section. This allows to form a conclusion that the electrochemical doping strategy leads to the introduction of iodine atoms across the entire layer thickness. The atomic concentration of iodine in I-TiO$_2$-KI equals 0.31 at. % and in I-TiO$_2$-HIO$_4$ sample equals 0.44 at. %.
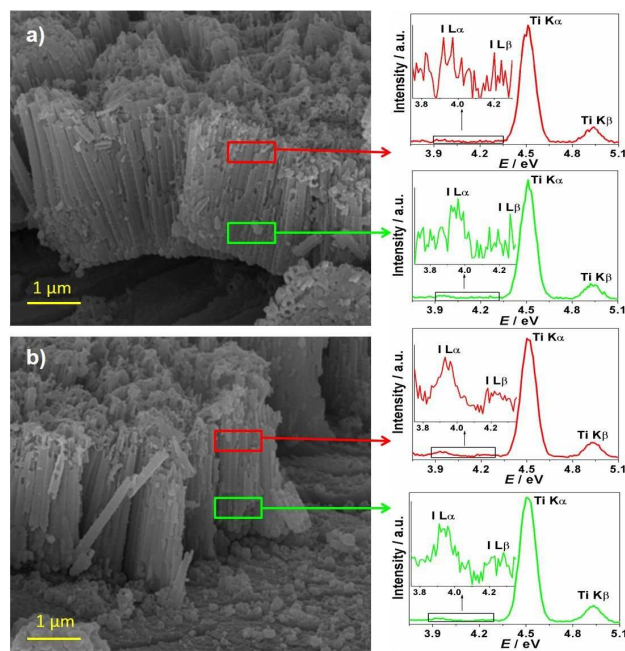

Fig. 3. Cross-section image of the titania nanotube layer of:
a) I-TiO$_2$-KI and b) I-TiO$_2$-HIO$_4$.

In Fig. 4a and 4b the absorbance curves and the Tauc plot are given, respectively. As it is typical for titanium dioxide materials, the highest absorbance was registered in the UV range. An additional wide absorption band is present in the visible range with maximum at 550 nm which could be attributed to the presence of sub-bandgap states resulting from the unusual structure of titania nanotube[12] or a considerable concentration of oxygen vacancies and other defects in the material[32]. In the case of doped samples, the absorbance in the range of 450 – 700 nm is more intensive in comparison to the undoped sample. As it was reported by Wang et al.,[33] different iodine forms can significantly affect the absorbance properties of TiO$_2$.

Basing on the Tauc plot, the bandgap energy values were determined and equaled 2.95 and 3.0 eV for I-TiO$_2$-KI, I-TiO$_2$-HIO$_4$, respectively, whereas for pure TiO$_2$ E_{bg} = 3.07 eV. Therefore, both doped materials were characterized by narrower bandgap energy in comparison to pure titania. Such a change in E_{bg} value is typically observed for iodine doped titania nanoparticles[34] and nanotubes as well[17]. It should also be noted that the bandgap energy value determined for undoped titania differs from typical E_{bg} known for anatase nanoparticles (3.20 eV).[35] It results from the presence of rutile, the oxide barrier layer at the interface Ti metal plate – titania nanotube layer. As it is known, the bandgap of rutile is lower than E_{bg} of anatase, thus the rutile phase at the interface shifts the absorption edge of the nanotube layer towards the visible range.

Furthermore, differences between the absorbance ability of the nanotubular film and nanoparticles are strongly connected to the oxide gradient raised during the thermal annealing process and the tube length.[9,36]
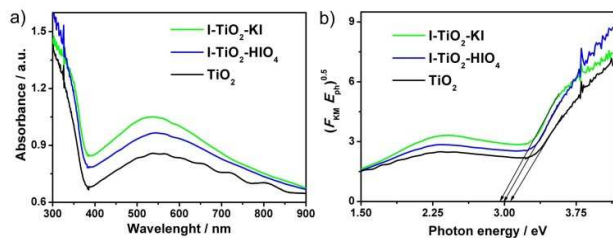
Fig. 4 a) Absorbance spectra and b) the Tauc plot for pure and doped titania.

The Raman spectra of pure TiO_2 and iodine doped titania are shown in Fig. 5. Raman spectra show five bands typical for the anatase crystalline phase: at about 144, 196, 391, 514 and 634 cm^{-1} which are indexed to $E_{g(1)}$, $E_{g(2)}$, B_{1g}, A_{1g} and $E_{g(3)}$ active modes, respectively. In general, the Raman spectra recorded for the undoped and iodine doped samples does not differ significantly, which indicates that the material has not changed structurally after the electrochemical treatment in iodine-containing electrolytes. However, a slight shift of $E_{g(1)}$ maximum from 143.28 cm^{-1} registered for pure TiO_2 to 144.12 cm^{-1} and 144.47 cm^{-1} for I-TiO_2-HIO_4, I-TiO_2-KI, respectively, is observed. The shift could result from bonding of iodine to TiO_2 or an increase of crystalline defects formed in the titanium dioxide framework due to the presence of iodine ions.[37] According to Choudhury et al.,[38] shifting of $E_{g(1)}$ peak towards higher wavenumbers is caused by the introduction of dopant atoms which disturb Ti-O-Ti bonds and generate oxygen vacancies.
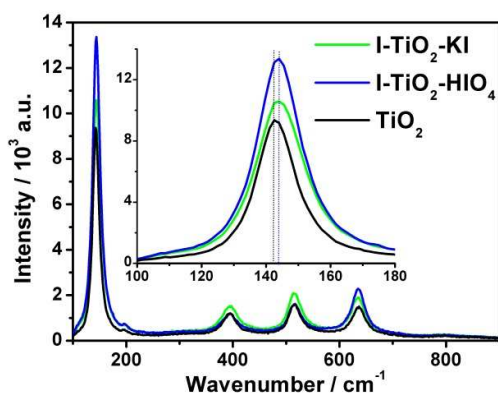
Fig. 5 Raman spectra of pure and iodine doped titania.

The photoluminescence spectra of all nanotubular layers are shown in Fig. 6. The broad band with a maximum at 530 nm (2.34 eV) can be clearly observed for all samples and can be identified as surface states[39] or as energy level at which deep trapped excitons can be located.[40] In general, the value of luminescence is strongly connected to the radiative recombination of excited electrons and holes, i.e. the higher intensity of photoluminescence, the higher

probability of electron-hole recombination. Among investigated materials, pure titania is characterized by the highest photoluminescence intensity which means that iodine doping participate in charge carrier separation[37] and significantly inhibit radiative recombination processes.[41] Thus, apart from the improved absorbance capability of I-TiO_2 samples, the presence of iodine dopant atoms also leads to an increase of generated current during illumination.
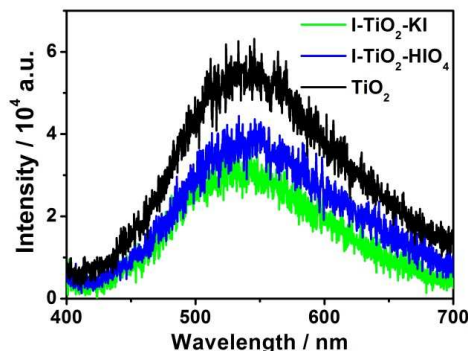
Fig. 6 Photoluminescence spectra of pure and I-doped samples.

The X-ray photoelectron spectroscopy allows to confirm iodine presence and to investigate the nature of elements in titania surface regions after the electrochemical doping procedure. Fig.7 shows the high resolution XPS spectra for each element present in the doped samples. The XPS spectra as well as the position of each maxima recorded for pure titania nanotubes were described in our previous report.[12] Table 1 summarizes the position of the deconvoluted peaks for doped nanotube arrays as well as for the undoped material. For all analyzed materials, the signals attributed to titanium, oxygen, carbon and iodine were detected. Additionally, for the I-TiO_2-KI sample, a weak signal at 292.33 eV assigned to potassium was found. It could remain in titania nanotubes after their electrochemical treatment in a solution containing KI salt. The atomic ratio of Ti:O:I is 1:2.57:0.080 and 1:2.48:0.063 for I-TiO_2-KI and I-TiO_2-HIO_4 samples, respectively.

**Table 1** The binding energy of core levels: I3$d_{3/2}$, Ti2$p_{1/2}$ Ti2$p_{3/2}$, O1s, C1s of elements present in doped and pristine titania nanotube arrays.

element	core level	I-TiO_2-KI [eV]		I-TiO_2-HIO_4 [eV]	TiO_2 [eV]
iodine	I3d3/2	617.07	618.4	618.6	-
	I3d5/2	628.46	629.88	630.09	-
titanium	Ti2p1/2	458.57		458.37	458.8
	Ti2p3/2	464.3		464.09	464.4
oxygen	O1sA	529.75		529.65	529.2
	O1sB	531.86		531.89	531.7
carbon	C1sA	284.59		284.56	284.7
	C1sB	286.19		285.95	286; 288.7

The region attributed to titanium was characterized as doublet: Ti2$p_{1/2}$ and Ti2$p_{3/2}$. The positions of Ti2$p_{1/2}$ are: 458.57 eV and

458.37 eV for I-TiO$_2$-KI and I-TiO$_2$-HIO$_4$ respectively, that can be assigned to Ti^{4+} oxidation state.[42] As it can be seen, the location of Ti2p peak found for both types of I-TiO$_2$ materials is shifted towards the lower binding energy value in comparison to Ti2p observed for pure TiO$_2$. The decrease of the Ti2$p_{3/2}$ binding energy may be due to the formation of the new chemical arrangement I-Ti-O, as proposed by Wang et al.[43] Iodine dopant is characterized by electronegativity below 0, thus a decrease in the electron density around Ti and the screening effect observed results in the increase of binding energy of Ti2$p_{3/2}$.

The XPS region attributed to O1s was fitted using two singlets: O1sA and O1sB (see Fig. 7b). They correspond respectively to lattice oxygen and surface bound hydroxyl group[44] or chemisorbed oxygen.[42] The signals attributed to oxygen in iodine doped titania are located at higher energy value compared to the adequate position of O1s for pure titania. Such a notable shift of O1s maxima could be due to a partial substitution of oxidic states.[45] A similar kind of conclusion had been derived for anionic doping of TiO$_2$ nanoparticles by nitrogen and carbon.[46]
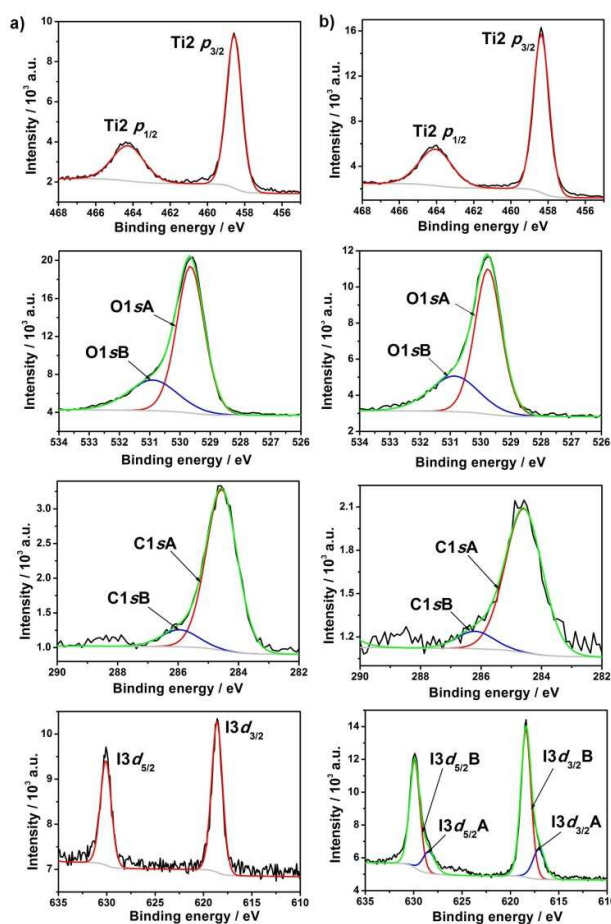
Fig. 7 High resolution XPS spectra recorded at the oxygen, titanium, carbon and iodine region for a) I-TiO$_2$-HIO$_4$ and b) I-TiO$_2$-KI samples.

Apart from titania and oxygen, the signal attributed to carbon was detected in all investigated samples. The carbon C1s region is formed by two singlets[47]. The highest carbon signal located at

284.59 eV (I-TiO$_2$-KI) or 284.56 eV (I-TiO$_2$-HIO$_4$) could be assigned to C-C bonds and is regarded as a contaminant adsorbed on titania surface[48]. Such carbon residues are typical for TiO$_2$ nanotubes that were formed in electrolytes containing organic solvents, e.g. ethylene glycol[49] or could be ascribed to possible carbon contamination from the instrument.[50] The next peak found at 286.19 eV or 285.95 eV for I-TiO2-KI and I-TiO2-HIO4 respectively corresponds to oxygen bond carbon.[51]

The XPS spectra of I3d region show a clear doublet with peaks located at c.a. 618 and 630 eV for both doped samples similarly to other I-TiO2 materials.[52,53] There were no detectable peaks attributed to I^{7+} or I^{5+} at the binding energy of about 624 eV reported by Su et al.[16] for I-TiO$_2$ doped nanotubes synthesized using periodic acid as iodine precursor. According to Shi et al.,[53] registered signals should be ascribed to negatively charged iodine species. Because iodine on 5+ or 7+ oxidation state exist in the form of iodate (IO$_3^-$) or periodate (IO$_4^-$) and ionic radius of I$^-$ (0.216 nm) is much larger than that of O^{2-} (0.124 nm) or Ti^{4+} (0.068 nm), the substitution of Ti^{4+} or O^{2-} ions in the lattice by I$^-$ would hardly be probable. Therefore, it is possible that I$^-$ species are dispersed on the tube surface or at the interstitial sites of the TiO$_2$ lattice. Nevertheless, the substitution of oxygen or titanium by any iodine species will significantly affect the anatase matrix[54].

As it can be seen, the I-bands recorded for I-TiO$_2$-KI were deconvoluted into two doublets, ascribed as: A (617.07 eV; 628.46 eV) and B (618.4 eV; 629.88 eV), whereas for I-TiO$_2$-HIO$_4$ single doublet (618.6 eV; 630.09 eV) was fitted. Until now, such deconvolution into two doublets was reported for iodine doped graphene oxide[55] or bismuth oxide.[56] According to Slimek et al.,[57] they could be attributed to the multitude of chemical bonds, including elemental iodine, polyiodide anion: I^{3-} and I^{5-} with respective binding energies at 618.9 eV and 619.7 eV. However, on the contrary to I-doped graphene oxide or graphene,[58] no Raman bands typical for I^{3-} (109 cm^{-2}) or I^{5-} (167 cm^{-1}) were registered. Additionally, Cabibil et al.[59] also consider signals near 620 eV as C-I bonding. On the other hand, the analysis of iodine spectra registered for non-stoichiometric BOI$_{1.5}$ was fitted with two sets of peaks similarly as in our case. One attributed to bulk iodine and another to I$^-$ from the excess of KI. Thus, because the presence of potassium traces was confirmed on the XPS survey spectra, the most likely interpretation of two doublets in the case of I-TiO$_2$-KI can be attributed to the interstitial iodine and iodine present in KI residues. Nevertheless, we could conclude that high resolution XPS alone is not sufficient to precisely determine the type of iodine bonding within titania nanotubular structure and further specification using e.g. EXAFS should be undertaken.

The mechanism of iodine doping induced by the presence of periodic acid that was used as dopant precursor was proposed by Li et al.[52] As it was reported, iodic acids form highly oxidative environment due to the presence of iodine with a high oxidation state characterized by high reactivity and ability to easily form multivalence iodine oxides: I$_2$O$_5$, I$_4$O$_9$. Such multivalence iodine species could accept oxygen atoms within the titania crystal lattice leading to the formation of the I-O-Ti arrangement that is with oxygen vacation. Here, oxygen vacancies are generated in the titania lattice, that is caused by the reduction process of periodic acid when iodine oxidation state of iodine (7+) is lowered to multi-

valence states. During the electrochemical reduction process taking place at an electrode covered with nanotube arrays and immersed in periodic acid solution, the electrons released are involved in the generation of oxygen vacancies and simultaneously the electrons induce reduction of Ti^{4+} to Ti^{3+}.

Reduction of periodic acid may proceed according to Lee et al.[60]:

$$H_5IO_6 + H^+ + e^- \rightarrow HIO_3^- + 3H_2O \quad (3).$$

Then, I^{5+} could be reduced to lower valence states[52]: $I^{5+} + 2e^- \rightarrow I^{3+}$ and/or $10I^{5+} + 10e^- \rightarrow 5I_2\uparrow$.

These multi-valence states act as electron scattering sites that may influence efficient separation of charge carriers[61]. As it was mentioned, the generation of oxygen vacancies: $O \rightarrow 1/2O_2 + V_o^{2+} + 2e^-$ takes place in parallel with the formation of the I-O-Ti bonds. In the case of the electrochemical process carried out in KI solution when 1.5 V is applied between the titania nanotubular anode and Pt mesh cathode, oxidation of iodide ions might proceed according to: $2I^- - 2e^- \rightarrow I_2$; $3I^- - 2e^- \rightarrow I_3^-$, $2I_3^- - 2e^- \rightarrow 3I_2$. Thus, triiodide and iodide ions and iodine molecules can also be involved in possible doping phenomena.

Electrochemical characterization

Cyclic voltammetry was performed to characterize materials in contact with the deareated electrolyte (pH = 7). In Fig. 8, CV curves registered both for pure and iodine doped materials. The working electrode was polarized from the rest potential in the anodic direction up to 1 V and back up to -1 V *vs.* Ag/AgCl/0.1M KCl. In general, the shape of CV curve is typical for titanium dioxide materials with a marginal capacitive current in anodic region (marked as A).[62,63] However, in the case of doped materials, the clear reduction peak marked as B at -0.2 V *vs.* Ag/AgCl/0.1M KCl is present that could be due to the presence of dopant atoms. According to Pelouchowa et al.,[64] this cathodic peak can be ascribed to the reduction of Ti^{4+} sites in TiO_2. As a result of the electrochemical reaction, the change in the electronic structure of TiO_2 takes place. This change is the formation of additional energy levels within the bandgap that significantly influences electrical conductivity as well as the optical properties of the material.[3] At more negative potential when compared to the location of area B, the hydrogen evolution process is initiated.
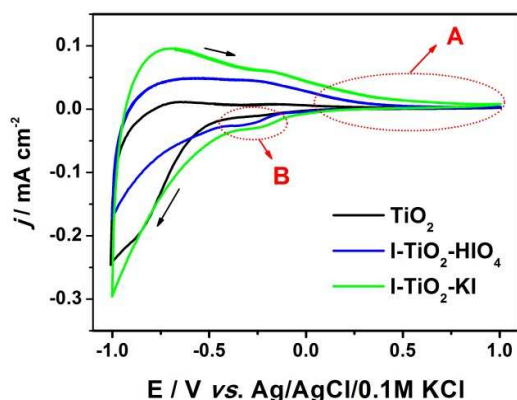
Fig. 8 Cyclic voltammetry curves recorded for doped and pristine TiO_2 immersed in 0.1M K_2SO_4, *v* = 50 mV/s.

Electrochemical impedance spectroscopy was used to determine the space charge layer capacitance. The impedance spectra were

recorded in the wide potential range, starting at the most anodic potential. The example impedance spectra is shown in Fig. 9a together with data points obtained from the fitting procedure. In order to analyze the collected spectra, the equivalent electric circuit (*EEQC*) was used: $R_e(CPE_1R_1)(CPE_2R_2Wo)$ (see Fig. 9b) similar to that proposed by Munoz et al.[65] The R_e element corresponds to the electrolyte resistance. The following arrangement of electrical elements: (CPE_1R_1) and $(CPE_2R_2W_0)$ connected in series is attributed to a compact oxide thin film and ordered nanotubular layer, respectively[65]. According to the approach proposed by Brug et al.,[66] the *CPE* element is not pure capacitance, due to inhomogeneity of the electrode, but a constant phase element characterized by impedance $Z = Q^{-1}(i\omega)^{-\alpha}$, where certain frequency dispersion α is taken into account. For the proposed fitting procedure, the value of α was in the range of 0.88 − 0.95. The CPE_2 element strongly depends on the potential applied, whereas no significant dependency on the potential was observed for CPE_2 value. The constancy of CPE_1 element could be a consequence of the small reactivity of the oxide barrier layer.[65]
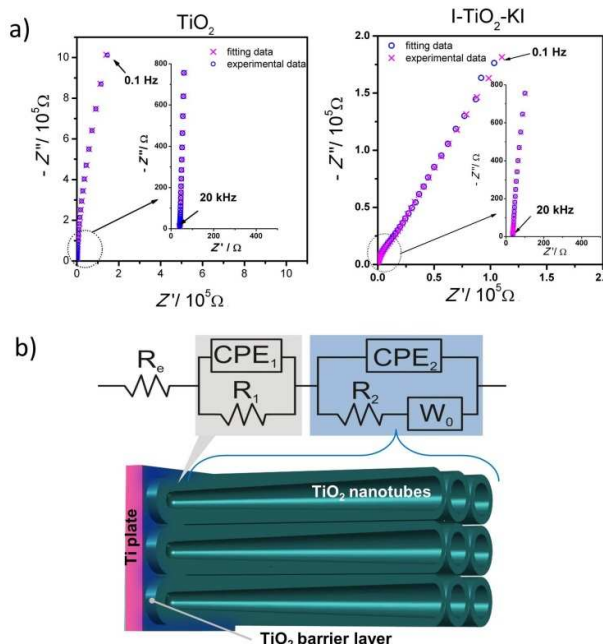
Fig. 9 a) An example of impedance spectra with experimental and fitting data obtained for TiO_2 and I-TiO_2-KI samples; b) The scheme of electric equivalent circuit used for impedance spectra fitting for all tested materials.

The Warburg open element (Wo), present in *EEQC* part attributed to the tubular layer, describes impedance of finite-length diffusion with reflective boundary as presented by this formula:

$$Z_{W_0}(\omega) = \frac{\omega_{or}}{\sqrt{\omega}}(1-j)\coth[W_{OC}\sqrt{j\omega}] \quad (4)$$

where W_{or} is equal to Warburg coefficient, W_{OC} = d/D$^{0.5}$. The use of finite length diffusion impedance to blocking electrode is necessary here to illustrate impedance related to charge transport within tubular TiO_2 bulk walls with bottom support down to blocking Ti support.

Moreover, an attempt has been made to use a second diffusion impedance reflecting charge transport within the space inside the pores filled with electrolyte, however this approach does not improve fitting results. It is believed that even at the lowest frequencies measured, the electrode material, especially TiO_2 barrier layer, does not allow the full penetration of electroactive species in the layer.[67]

Impedance data was used for further analysis using the Mott-Schottky relation which is expressed as:

$$\frac{1}{C^2} = \left(\frac{2}{q\varepsilon\varepsilon_0 N_D}\right)\left(E - E_{fb} - \frac{kT}{q}\right) \quad (5)$$

where C is areal capacity of the space charge layer, q – elementary charge, ε_0 - vacuum permittivity, ε - dielectric constant, N_D – concentration of donors, E – applied external bias, E_{fb} – flat-band potential, k – Boltzmann's constant, T- absolute temperature. The extrapolation to $C^{-2} = 0$ allows flat band potential determination whereas the doping level N_D can be calculated from the slope of the Mott-Schottky plot. As it is known, high concentration of multiple donor levels within the bandgap can cause indirect tunneling of electrons through the semiconductor, resulting in a variation of the slope with the frequency. Because of this phenomenon, instead of straight calculation of capacitance basing on relation: $C_{sc} = 1/2\pi Z''f$,[68] the C_{sc} value obtained from the fitting procedure was taken for the Mott-Shottky analysis. Basing on the dependence of CPE_2 value upon the applied potential, the capacitance of titania nanotubular layer was attributed to space charge capacitance that was required for preparation of the Mott-Schottky plot shown in Fig. 10. Following the relationship, a plot C^{-2} *vs.* E for a semiconducting material in the absence of deep-level electronic states is linear over the range of potentials where a depletion layer is formed. However, two regions characterized by different linear relations between C^{-2} *vs.* E are observed here and marked as red and gray lines. Such changes in the run of the Mott-Shottky function were interpreted as an intrinsic TiO_2 electronic state model rather than a geometric effect.[65] According to Bonham et al.,[69] deviations form linear relationship are commonly attributed to the influence of potential dependent charging of surface or bulk states. On the other hand, it could be found that a geometric factor such as tube length and wall thickness also plays a crucial role[9] and is strongly connected to the electronic structure. As it was reported by Wang et al.[70] and Yasuda et al.,[31] the distribution of net oxygen ions O^{2-} concentration is irregular at the cross-section of the tube and at the same moment the decrease of the tube wall thickness from the base up to the surface of tubular layer is observed. Therefore, layers composed of TiO_2 nanotube arrays are characterized by inhomogeneous distribution of different oxide composition (e.g. Ti_2O_3, TiO) that could result in a complex impedance response. Although an impedance analysis taking into account too many factors will not give us any clear information, the described phenomenon connected to changes in morphology and O^{2-} distribution should be kept in mind.
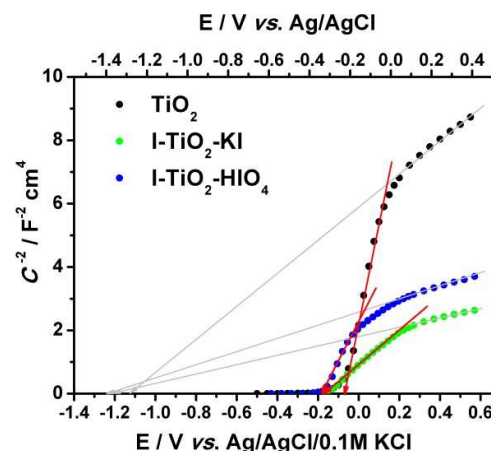
Fig. 10. The Mott-Schottky plot for pure and iodine doped titanium nanotube array layers, C calculated from CPE_2 taking into account α value.

According to the Munoz approach, the flatband potential determined on the intercept of the Mott-Schottky function (in the range from +0.15 to -0.2 V vs. Ag/AgCl/0.1M KCl) for pure titania is equal to -0.07 V *vs.* Ag/AgCl/0.1M KCl whereas E_{fb} for doped materials equals -0.16 V and -0.17 V *vs.* Ag/AgCl/0.1M KCl for I-TiO_2-HIO_4 and I-TiO_2-KI respectively. Taking into account the relation of C^{-2} *vs.* E in the positive range (from 0.15 V to 0.6 V *vs.* Ag/AgCl/0.1M KCl), the flatband potential will be much more negative but still the E_{fb} value for I-TiO_2 will be catholically shifted in comparison to E_{fb} determined for pure titania. According to Lee et all, presenceofdopand can raise the conduction band edge[71]. As it was mentioned above, the non-linear behavior of the Mott-Schottky plot could result from multiple donor levels that are ionized one after another[72]. However, we should also take into account the fact that proper flat band determination can be made based on spectra collected at potentials more positive than and close to the flatband potential to avoid modification of conductive properties. As it was shown on the cyclic voltammetry curves, in the case of iodine doped materials, the reduction process takes place near -0.2 V *vs.* Ag/AgCl/0.1M KCl and, in consequence, another element in *EEQC* attributed to the faradaic reaction should be introduced. Thus, data points on the Mott-Schottky plot present in the vicinity of reduction reaction should be interpreted carefully. Nevertheless, the determined flatband potential basing on C^{-2} *vs.* E relation in the range of 0.15 to -0.2 V *vs.* Ag/AgCl/0.1M KCl is reasonable and fits the range of potentials in which E_{fb} for other nanotubular TiO_2 layer was found.[73,74,75]

In-situ spectroelectrochemical studies

The application of spectroelectrochemical measurements involving UV-Vis spectroscopy together with simultaneous electrochemical measurements allows determination of the potential at which the initiation of electron injection to the available energy electron state occurs. The usage of a diffuse reflectance accessory instead of a transmission cell, broadens the UV-Vis in-situ spectroelectrochemistry application to non-transparent materials and is not influenced by the light scattering properties.

In general, for titania materials, absorbance enhancement observed in the visible range is attributed to the increase in electron density

in the conduction band.[76] A more detailed analysis of absorbance spectra recorded for TiO_2 nanotube arrays can be found in the previous section. As mentioned above, the absorbance maximum in the visible range for pure as well as for iodine doped samples was observed at 550 nm. Therefore, in analogy to the procedure proposed by Fritzmaurice,[76,27] for semitransparent electrode, the change of the reflectance value upon applied potential was monitored at wavelength at which the maximum in absorbance was registered. In Fig. 11, the changes in reflectance at λ = 550 nm for pure TiO_2 and iodine doped TiO_2 at simultaneous changes in working electrode potential are shown.
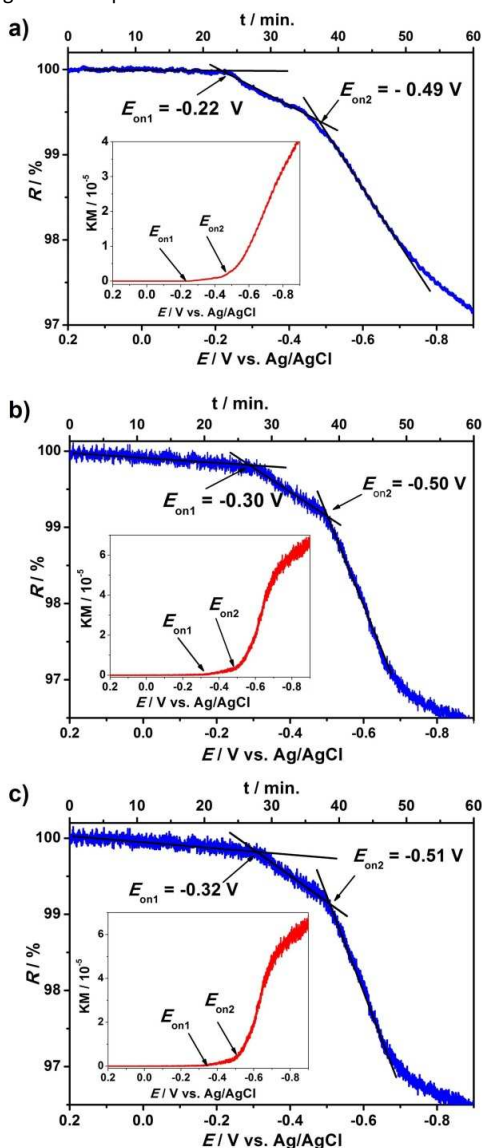
Fig. 11 Relative reflectance measured as 550 nm as a function of applied potential for a) pure TiO_2, b) I-TiO_2-KI and c) I-TiO_2-HIO$_4$, inset: reflectance converted to the Kubelka-Munk function.

Additionally as the inset, transformation of reflectance into Kubelka-Munk function is given. The potential, at which the electron trapping process is initiated - E_{on1}, can be determined

directly as the onset of reflectance changes or after recalculation - from Kubelka-Munk plot. In the case of pure titania, the onset of reflectance change was registered at -0.22 V vs. Ag/AgCl (-0.062 V vs. Ag/AgCl/0.1MKCl), whereas E_{on1} for I-TiO_2-KI and I-TiO_2-HIO$_4$ equals -0.30 and -0.32 V vs. Ag/AgCl respectively (-0.142 V and -0.162 V vs. Ag/AgCl/0.1M KCl). The value of E_{on1} is assigned either to the flatband potential or the Fermi level.[28] In other words, it describes the ability of materials to accept electrons. Because the onset potential observed for iodine doped titania is catholically shifted, they are characterized by improved capability towards electron acceptance. It should be noted that apart from the E_1 onset potential, an additional rapid change in the run of reflectance changes vs. applied potential is observed. Such shape is associated with filling in trap states in the semiconductor electrode located either in the bulk, at grain boundaries or at the semiconductor/electrolyte interface.[26] Trapping at grain boundaries is a possibility, however, trapping of electrons in surface states will most likely give rise to color changes at negative potentials.[77] Thus, subsequent charge injection upon polarization yields the number of accumulated electrons as a function of the electrode potential applied during cathodic polarization.

The E_{on1} value determined by in-situ spectroelectrochemical measurements is very similar to the flatband potential value determined on the basis on the Mott-Schottky plot. Such consistency can be regarded as a strong Fermi level pinning, connected to the high concentration of surface states that causes matching between E_f and E_{on1} values[78].

Therefore, apart from the electrochemical impedance spectroscopy measurement, in-situ spectroelectrochemical approach can be regarded as a useful method for E_{fb} estimation. Further cathodic polarization leads to a subsequent decrease in relative reflectance and a clear change of the slope appears at the potential E_{on2} - the same place at which the surface species undergo a faradaic reaction, see Fig. 8.

Photoactivity

Linear voltammetry (LV) was used to show magnitude of photocurrent generated under different applied potential to the titania electrode exposed to the UV-vis radiation of 100 mW cm^{-2}. The photoelectrochemical behavior dependent on the applied potential of pure and iodine doped TiO_2 is presented in Fig. 12. In the case of doped materials, a significant increase in photocurrent compared to pure titania nanotubes is recorded.
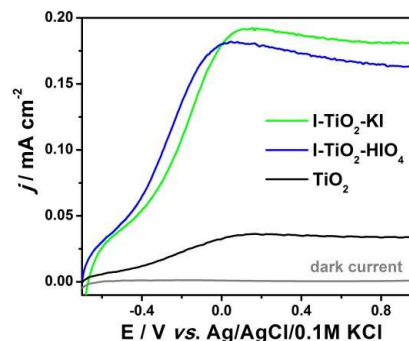
Fig. 12 Linear voltammetry curves registered for iodine doped and pure titanium dioxide nanotube arrays under UV-vis illumination.

The positive influence of a dopant is very likely due to the decrease of recombination processes and improved absorbance in the visible light as observed for other types of non-metal doped nanotube arrays.[79,80]

The chronoamperometry measurements facilitate the determination of the photocurrent retention at a constant potential and photoelectrode stability. Fig. 13 presents the transient photocurrent response of pure and iodine doped TiO_2 nanotube arrays by on-off cycles registered under UV-vis and vis irradiation periods. The curve shows that the current rapidly increased and decreased when the radiation was switched on and off, respectively. The lack of steady current diminution suggests that the materials exhibit photocorrosion-resistance. Table 2 presents the values of photocurrent density registered after 10 min. of measurements and the ratios of respective photocurrents between the pure and doped TiO_2 nanotubes. The highest saturated photocurrent was observed for $I-TiO_2$-KI reaching 155.2 $\mu A\ cm^{-2}$ and 3.1 $\mu A\ cm^{-2}$ under UV-vis and vis illumination, respectively. Thus, the photocurrents were 6.06 and 5.07 times higher than the current registered for undoped TiO_2 under the same light conditions. Despite the fact that photocurrent for $I-TiO_2$-HIO_4 is lower in comparison to $I-TiO_2$-KI, the enhancement on a level of about 5 is still an impressive achievement that has not be reached for other non-metal doped titania nanotubes.[24,77,81]
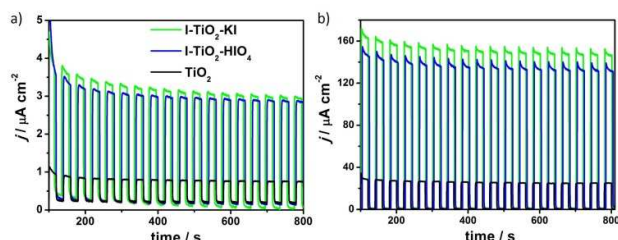
Fig. 13 Amperometric current density - time curves at an applied potential of 0.5 V vs. Ag/AgCl/0.1M KCl registered under a) vis and b) UV-vis irradiation.

Table 2. The photocurrent values registered for pure and I-doped TiO_2 under vis and UV-vis irradiation after 500 s of measurement. For each photoelectrode, the photocurrent ratio between the doped and pure TiO_2 is given in brackets.

sample	I_{ph} UV-vis / 10^{-6} A cm^{-2}	I_{ph} vis/ 10^{-7} A cm^{-2}
$I-TiO_2$-KI	155.2 (× 6.06)	30.9 (× 5.07)
$I-TiO_2$-HIO_4	142.4 (× 5.56)	28.7 (× 4.7)
TiO_2	25.6	6.1

Photocatalytic properties

The photocatalytic activity of pure and iodine doped TiO_2 nanotubes was investigated on the basis of the degradation progress of methylene blue (MB) as a model organic pollutant under UV-vis illumination. Fig. 14 presents the photocatalytic degradation of MB with an immersed titanium plate covered by TiO_2, $I-TiO_2$-KI and $I-TiO_2$-HIO_4. For comparison, a blank experiment under UV-vis irradiation without any sample was also performed. The slight decoloration of methylene blue solution is caused by a direct photolysis process induced by highly reactive radical species

formed in the presence of irradiation.[82] After a 2h illumination in the presence of undoped titania nanotubes, the degradation of methylene blue reached 31%, whereas the degradation efficiency of 71% and 65% was observed for $I-TiO_2$-KI and $I-TiO_2$-HIO_4, respectively. It is evident that the degradation of MB has been improved due to the doping of titania nanotubes with iodine which extends the absorption edges to the visible light region. In addition, the enhanced photocatalytic activity of doped titania nanotubes can be attributed to the more effective separation of the photogenerated electrons and holes. It is noteworthy that the application of the photocalalyst in the form of a solid plate immersed in contaminated fluid is advantageous in comparison to the common use of a catalyst suspension.
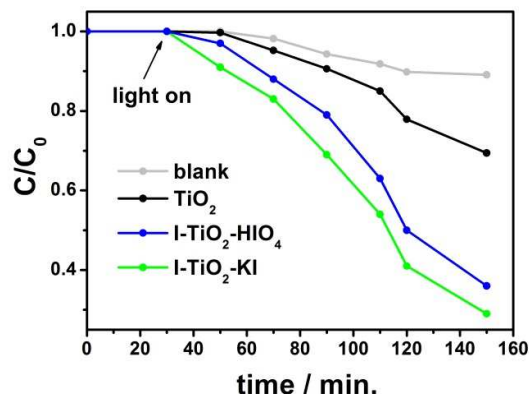
Fig. 14 Photocatalytic performance of the obtained samples under UV-vis illumination.

Conclusions

A simple method was proposed and optimized for the fabrication of photoactive and stable titania nanotube arrays doped with iodine. It was found that the electrochemical treatment in electrolyte containing iodine precursor (KI or HIO_4), as an additional step after formation of titania nanotube arrays via anodization, does not affect their tubular architecture. All types of obtained materials formed uniform layers composed of ordered nanotube arrays with 2.2 μm length and 95 nm of internal diameter. The presence of iodine species was confirmed and investigated by the X-ray photoelectron spectroscopy technique. Iodine-doped samples were characterized by lower bandgap energy and decrease of photoluminescence in comparison with pure titania. The measurements carried out under sample irradiation showed that iodine doping radically improved photocatalytic activity as well as the generation of photocurrent. After 2h of the photodegradation process for $I-TiO_2$-KI and $I-TiO_2$-HIO_4 materials, the amount of methylene blue remaining in the solution respectively equaled 29% and 35% of its initial concentration, whereas when TiO_2 was used as photocatalyst, it was equal to 69%. The enhancement of the current registered under UV-vis irradiation (100 mW/cm²) for iodine doped titania: $I-TiO_2$-KI and $I-TiO_2$-HIO_4 is 6.06 and 5.56 times higher than pure TiO_2. Furthermore, an investigation using the electrochemical impedance spectroscopy and in-situ UV-vis

spectroelectrochemical studies showed that electrochemical doping procedure induces noticeable changes of the electrochemical activity. This manifests as a different slope of the Mott-Schottky plot for doped and pure titania as well as a shift of the onset potential at which a decrease in reflectance is registered.

In summary, because of the highly improved photoactivity of the doped materials when compared to pristine TiO_2, iodine doped titania nanotubes show good potential for application as photoelectrodes in dye sensitized solar cells or for sustainable photocatalytic degradation of environmental hazardous substances. However, further studies concerning detailed investigations of the nature of iodine need to be carried out.

Acknowledgements

References

1   P. Roy, S. Berger, P. Schmuki, *Angew Chimie Inter,* 2011, **50**, 2904.

2   G.K. Mor, O.K. Varghese, M. Paulose, K. Shankar, C.A. Grimes, *Sol Energy Mater Sol Cell*, 2006, **90**, 2011.

3   J.M. Macak, H. Tsuchiya, A. Ghicov, K. Yasuda, R. Hahn, S. Bauer, P. Schmuki, *Curr. Opp. in Solid State Mater. Sci*, 2007, **11**, 3.

4   D. Kowalski, D. Kim. P. Schmuki, *NanoToday*, 2013, **8**, 235.

5   G.D. Sulka, J. Kapusta-Kolodziej, A. Brzozka, M. Jaskuła, *Electrochim Acta*, 2013, **104**, 526.

6   H. He, C. Liu, K.D. Dubois, T. Jin, M.E. Louis, G. Li, *Ind Eng. Chem Res*, 2012, **51**, 11841.

7   J. Lee, D.H. Kim, S.H. Hong, J. Y. Jho, *Sensors Actuators B Chem*, 2011, **160**, 1494.

8   H.F. Zhuang, C.J. Lin, Y.K. Lai, L. Sun, J. Li, *Environ. Sci. Technol.*, 2007, **41**, 4735.

9   C.A. Grimes, G.K. Mor, *Use of TiO_2 nanotube arrays for biological applications, TiO_2 nanotube arrays*, 2009 Springer, p. 285-314

10 A. Matsuda, S. Sreekantan, W. Krengvirat, *J Asian Ceram Soc.,* 2013, **1,** 203.

11 S. Kurian, H. Seo, H. Jeon, *J Phys Chem C, 2013,* **117**, 16751.

12 K. Siuzdak, M. Szkoda, M. Sawczak, A. Lisowska-Oleksiak, *New J Chem*, 2015, **39,** 2741.

13 X. Tang, D. Li, *J Phys Chem C,* 2008, **112**, 5405.

14 Y. Zhang, W. Fu, H. Yang, S. Liu, P. Sun, M. Yuan, D. Ma, W. Zhao, Y. Sui, M. Li, Y. Li, *Thin Solid Films*, 2009, **518**, 99.

15 G.G. Bessegato, J. C. Cardoso, M. V.B. Zanoni, *Catal. Today*, 2015, **240**, 100.

16 Y. Su, Y. Xiao, X. Fu, Y. Deng, F. Zhang, *Mater Res Bull*, 2009, **44**, 2169.

17 Y. Su, Y. Xiao, Y. Du, S. Fu*, Chin. Sci. Bull*, 2010, **55,** 2136.

18 A.W. Bott, *Curr. Separat.*, 1998, **17**, 87.

19 J.O'M. Bockris, S.U.M. Khan, *Surface Electrochemistry, a Molecular Level Approach, Plenum Press*, New York 1993, p170-173.

20 A.M. Roy, G.C. de. N. Sasmal, S.S. Bhattacharyya, *Int. J. Hydrogen Energy*, 1995, **20**, 627.

21 M.D. Ward, J.R. White, A.J. Bard, *J. Am. Chem. Soc*., 1983, **105**, 27.

22 R. Beranek, H. Kisch, *Electrochem. Comm*, 2007, **9**, 761.

23 M. Hepel, S. Hazelton, *Electrochim. Accta,* 2005*, **50**,* 5278.

24 X. Cheng, H. Liu, Q. Chen, J. Li, P. Wang, *Electrochim. Acta*, 2013, **103**, 134.

25 G. Boschloo, D. Fitzmaurice, *J. Phys Chem B*, 1999, **103**, 7860.

26 G. Boschloo, D, Fritzmaurice, *J Phys Chem B*, 1999, **103,** 2228.

27 G. Redmond, D. Fitzmaurice, *J. Phys Chem*, 1993, **97,** 1426.

28 E. Świętek, K. Pilarczyk, J. Derdzińska, K. Szaciłowski, W. Macyk, *Phys. Chem. Chem. Phys*., 2013, **15,** 14256.

29 A.S.R. Bondarenko, G.A. Ragoisha, *Inverse Problem In Potentiodynamic Electrochemical Impedance, in: A.L. Pomerantsev (Ed.) Progress in Chemometrics Research, Nova Science Publishers*, New York, 2005, 89-102.

30 L. Lu, B.H. Brown, D.C. Barber, A.D. Leathard, *Physiological Measurement*, 1995, **16**, A39.

31 K. Yasuda, P. Schmuki, *Electrochim Acta*, 2007, **52,** 4053.

32 Y. Li, Y.Jiang, S. Peng, F. Jiang, *J Hazard Mater,* 2010, **182**, 90.

33 W. Wang-an, S. Qian, W. Yu-ping, C. Jin-li, L. Guo-qing, P. Pan-yang, *Appl. Surf. Sci.*, 2011, **257**, 3688.

34 A. Lisowska-Oleksiak, K. Szybowska, V. Jasulaitiene, *Electrochim. Acta*, 2010, **55**, 5881.

35 W.J. Yin, S. Chen, J.H. Yang, X.G. Gong, Y. Yan, S.H. Wei, *Appl. Phys Lett.,* 2010, **96**, 221901..

36 K.G. Ong, O.K Vargheseand G.K Mor and CA Grimes, *J. Nanosci. Nanotechnol.* 2005, **5** ,1.

37 S. Bagwasi, B. Tian, F. Chen, F. Chen, J. Zhang*, Appl. Surf. Sci*., 2012, **258**, 3927.

38 B. Choudhury, M. Dey and A. Choudhury, *Inter. Nano Lett.* 2013, **3**, 25.

39 L. Forss and M. Schubnell, *Appl. Phys. B* 1993, **56**, 363.

40 J.H. Jang, K.S. Jeon, T.S. Park, K.W. Lee and M. Yoon, *J. Chin. Chem. Soc*. 2006, **53**, 123.

41 E. Wang, T. He, L. Zhao, Y. Chen, Y. Cao, *J. Mater. Chem*.,2011, **21**, 144.

42 Q. Zhang, Y. Li, E.A. Ackerman, M. Gajdardziska-Josifovska, H. Li, *Applied. Catal. A: General*, 2011, **400,** 195.

43 Y. Wang, J. Ren, G. Liu, P. Peng, *Mater. Chem. Phys*., 2011, **130**, 493.

44 Y. Ma, J.W. Fu, X. Tao, X. Li, J.F. Chen, *Appl. Surf Sci.,* 2011, **257**, 5046.

45 S. Anandan, K. Kathiravan, V. Murugesan, Y. Ikuma, *Catal. Comm*., 2009, **10**,1014.

46 J. Yang, H. Bai, X. Tan, J. Lian, *Appl. Surf. Sci*, 2006, **253**, 1988.

47 A.L. Cui, T.J. Wang, Y. Jin, *Eng. Chem. Metal*., 1999, **20**, 178.

48 T.T. Isimjan, A. El Ruby, S. Rohani and A.K. Ray, *Nanotechnology* 2010, **21**, 55706.

49 J. Zhang, B. Gao, Q. Gan, J. Xia, Y. Cao, J. Wang, K. Huo, *Chem. Rapid Comm*., 2014, **2**, 29.

50 Y. Li, G. Ma, S.Peng, G.Lu, S. Li, *Appl Surf Sci* , 2008, 254,6831.

51 J.H. Yun, R.J. Wong, Y.H. Ng, A. Du, R. Amal, *RSC Advances*, 2012, **2**, 8164.

52 W. Li, R. Liang, A. Hu, Z. Huang, Y. Norman Zhou, *RSC Adv*., 2014, **4**, 36959.

53 N. Shi, X. Li, T. Fan, H. Zhou, J. Ding, D. Zhang, H. Zhou, *Energy Environ Sc***i**, 2011, **4**, 172.

54 K. Yang, Y. Dai, B. Huang, M.H. Whangbo, *Chem. Mater*., 2008, **20**, 6528.

55 J. Wang. B. Li, T. Ni, T. Dai, Y. Lu, *Composites Sci Technol*, 2015, **109**, 12.

56 X. Zhang, L. Zhang, *J. Phys.Chem C*, 2010, **114**, 18198.

57 P. Slimek, K. Klimowa, D. Sedmidubsky, O. Jankovsky, M. Pumera, Z. Sofer, *Nanoscale,* 2015, **7**, 261.

58 G. Kalita, K. Wakita, M. Takahashi, M. Umeno, *J Mater Chem,* 2011, **21**, 15209.

59 H. Cabibil, H. ihm, *J.M. White, Surf Sci,*2000, **447**, 91.

60 B. Lee, D.J. Duquette, R. J. Gutmann, *Chemical –mechanical polishing of copper with model slurries, Electrochemical science and Technology of Copper* 2002.

61 W.Y. Su, Y.F. Zhang, Z.H. Li, L. Wu, X.X. Wang, J.Q. Li, X.Z. Fu, *Langmuir*, 2008, **24**,3422.

62 H. Du, Y. Xie, C. Xia, W. Wang, F. Tian, *New J. Chem*., 2014, **38**, 1284.

63 H. Yu, J. Ma, Y. Zhang, X. Zhang, W. Shi, *Electrochim. Acta*, 2011, **56**, 6498.

64 H. Pelouchova, P. Janda, J. Wber, L. Kavan, *J. Electroanal Chem*, 2004, **566**, 73.

65 A.G. Munoz, Q. Chen, P. Schmuki, *J Solid state Electrochem*, 2007, **11**, 1077.

66 G.J. Brug, A.L.G. Van Den Eeden, M. Sluyters-Rehbach and J.H. Sluyters, *J. Electroanal. Chem*., 1984, **176**, 275.

67 A.J. Roberts, R.C.T. Slade, *ECS Translactions*, 2010, **28**, 33.

68 A. Hagfeldt, U. Bjorkstein, M. Gratzel, *J Phys Chem*., 1996, **100**, 8045.

69 D.B. Bonham, M.E. Orazem, *J Electrochem Soc*, 1992, **139**, 127.

70 Zhou, *IEE Trans Nanotechnol*, 2015, **14**, 113.

71 Y. Li, Y. Xiang, S. Peng, X. Wang, L. Zhu, Electrochim Acta, 2013, 87, 794.

72 E.J. Lee, S.I. Pyun, *J. Appl. Electrochem*, 1992, **22**, 156.

73 I. Hanzu, T. Djenizian, P. Knauth, *J. Phys Chem C*. 5989.

74 Y. Tan, S. Zhang, K. Liang, *Nanoscale Res Lett*., 2014, **9**, 67.

75 R. Beranek, H. Tsuchiiya, T. Sugishima, J.M. Macak, L. Taveira, S. Fujimoto, H. Kisch, P. Schmuki, *Appl. Phys. Lett.*, 2005, **87**, 243114.

76 G. Rotherberger, D. Fritzmaurice, M. Gratzel, *J Phys. Chem*, 1992, **96**, 5983.

77 F. Cao, G. Oskam, P.C. Searson, J.M. Stipkala, T.A. Heimer, F. Farzad, G. J. Meyer, *J. PhysChem*, 1995, **99**, 11974.

78 T. Berger, J.A. Anta, V. Morales-Florez, J*. Phys Chem C*, 2012, **116**, 11444.

79 S. Li, L. Yang, S. Xu, S. Luo, Q. Cai, *Electrochem. Comm*., 2009, **11**, 1748.

80 H. Li, J. Xing, Z. Xia, J. Chen, *Electrochim. Acta*, 2014, **139**, 331.

81 S. Liu, L. Yang, S. Xu, S. Luo, Q. Cai, *Electrochem. Comm.* 2009, **11**, 1748.

82 J. Li, N. Lu, X. Quan, S. Chen, H. Zhao, *Ind. Eng. Chem. Res.*, 2008, **47**, 3804.